A Comparative Study of Pellet-Based Extrusion Deposition of Short, Long, and Continuous Carbon Fiber-Reinforced Polymer Composites for Large-Scale Additive Manufacturing

John M. Pappas[1]
Mechanical and Aerospace Engineering,
Missouri University of Science and Technology,
Rolla, MO 65409
e-mail: jmpn47@mst.edu

Aditya R. Thakur[1]
Mechanical and Aerospace Engineering,
Missouri University of Science and Technology,
Rolla, MO 65409
e-mail: artt4b@mst.edu

Ming C. Leu
Mechanical and Aerospace Engineering,
Missouri University of Science and Technology,
Rolla, MO 65409
e-mail: mleu@mst.edu

Xiangyang Dong[2]
Mechanical and Aerospace Engineering,
Missouri University of Science and Technology,
Rolla, MO 65409
e-mail: dongxi@mst.edu

Pellet-based extrusion deposition of carbon fiber-reinforced composites at high material deposition rates has recently gained much attention due to its applications in large-scale additive manufacturing. The mechanical and physical properties of large-volume components largely depend on their reinforcing fiber length. However, very few studies have been done thus far to have a direct comparison of additively fabricated composites reinforced with different carbon fiber lengths. In this study, a new additive manufacturing (AM) approach to fabricate long fiber-reinforced polymer (LFRP) was first proposed. A pellet-based extrusion deposition method was implemented, which directly used thermoplastic pellets and continuous fiber tows as feedstock materials. Discontinuous long carbon fibers, with an average fiber length of 20.1 mm, were successfully incorporated into printed LFRP samples. The printed LFRP samples were compared with short fiber-reinforced polymer (SFRP) and continuous fiber-reinforced polymer (CFRP) counterparts through mechanical tests and microstructural analyses. The carbon fiber dispersion, distribution of carbon fiber length and orientation, and fiber wetting were studied. As expected, a steady increase in flexural strength was observed with increasing fiber length. The carbon fibers were highly oriented along the printing direction. A more uniformly distributed discontinuous fiber reinforcement was found within printed SFRP and LFRP samples. Due to decreased fiber impregnation time and lowered impregnation rate, the printed CFRP samples showed a lower degree of impregnation and worse fiber wetting conditions. The feasibility of the proposed AM methods was further demonstrated by fabricating large-volume components with complex geometries. [DOI: 10.1115/1.4049646]

Keywords: additive manufacturing, carbon fiber-reinforced polymer, long fiber reinforcement, fiber length, high deposition rate, advanced materials and processing, rapid prototyping and solid freeform fabrication

Introduction

Thermoplastic polymers have been of growing interest in applications over a large spectrum of consumer and industrial products due to their manufacturing flexibility and recyclability. Specifically, fiber-reinforced thermoplastic composites are being extensively used due to the strength, modulus, and weight advantage they provide over their polymer counterparts [1,2]. With increasing demands, several manufacturing processes that facilitate large-scale, customized fabrication of fiber-reinforced composite parts have been developed, including additive manufacturing (AM), machining, casting, extrusion, and molding. Molding is one of the most widely used fabrication approaches for large-scale, tight-tolerance, complex fiber-reinforced composite parts but at high manufacturing costs [2]. It is worth noting that automated fiber placement (AFP) and automated tape placement (ATP) are another manufacturing methods with high potentials for fabrication of fiber-reinforced composite parts, which allow continuous fiber reinforcement [3,4]. However, capital expenditures for computer-driven, automated equipment can be significant [5]. Moreover, depending on the materials, the structures may require post-deposition curing via heat, vacuum, or autoclave processing, which may further increase the production cost [6,7]. The need for molds further lowers customizability of the fabricated composite structures [8]. While flexible molds or pin-based molds help in controlling the production costs associated with molds [9] or even mold-less composite manufacturing for AFP with recent advancements [10,11] may become feasible, there are still manufacturing challenges associated with the cost and manufacturing complexity due to requirements for curing, post-processing, and specialized tooling.

Additive manufacturing approaches, including fused filament fabrication (FFF), offer flexible, tool-less, and mold-less fabrication processes [12]. Until recently, due to low printing speeds and long fabrication time, AM was mainly limited to printing low-volume components. Advancements in large-scale additive manufacturing (LSAM) have addressed these shortcomings to a certain degree [13]. Previous studies showed that LSAM at high material deposition rates allowed additive fabrication of large-volume parts without excessive printing time, while reinforcing with fiber additives helped in elevating mechanical performances of the printed parts.

The mechanical and physical properties of fibrous composites largely depend on the orientation and aspect ratio of reinforcing

[1]These authors contributed equally to this work.
[2]Corresponding author.
Manuscript received September 13, 2020; final manuscript received December 20, 2020; published online March 5, 2021. Assoc. Editor: Martine Dubé.

fiber as well as interfacial bonding [14–17]. Increasing fiber length typically promotes mechanical properties [1,18–20], but increases difficulties of composite processing [1,15]. Nano- and micron-sized [21–23], short [24,25], and continuous fiber-reinforced composites using filament-based FFF approaches [26–30] have been extensively studied. The material costs in these manufacturing approaches are relatively high as they need to use specialized fiber-reinforced filaments as raw material for fabrication [31]. Low-cost AM of continuous fiber-reinforced polymer (CFRP) using thermoplastic pellets and continuous fibers has been recently investigated [16,32]. CFRP filaments were first in situ prepared from continuous fibers via micro-screw extrusion and then directly used by FFF machines to print CFRP parts. However, these processes were impractical for fabrication of large-volume components, which usually take several hours, or even days, to finish due to low deposition rates (about 0.5 g/min) [29,33]. Meanwhile, with high material deposition rates, pellet-based extrusion deposition of short fiber-reinforced polymer (SFRP) has been extensively used for LSAM [34,35]. To the best of our knowledge, very few previous studies can be identified on comparing composites reinforced with continuous, long, and short carbon fibers used for LSAM.

Typically, CFRP is mechanically superior as it offers longer reinforcing fiber lengths [27–30]. However, difficulties in processing of fiber-reinforced composites also increase with an increase in fiber length [1]. Inadequate impregnation poses challenges in achieving high-quality CFRP and necessitates post-processing to improve fiber-matrix wetting and take advantage of continuous fiber reinforcement in mechanical performance [16,36,37]. Previous studies showed that fiber-matrix wetting was affected by processing parameters including melting temperature [29] and laser pre-heating conditions [17], attributed to thermoplastic melt flowability and viscosity. It was found that high pressure, and shear-thinning effect [16] would also promote fiber wetting conditions. Meanwhile, pre-impregnation [17] and fiber sizing treatment [38] would improve fiber-matrix interfacial performance. In comparison, long fiber-reinforced polymer (LFRP) with high-aspect ratio fibers can provide improved mechanical performance, almost comparable to CFRP samples, while minimizing fabrication limitations associated with CFRP. Additive fabrication of CFRP samples is often limited by their printability with a relatively narrow range of proper printing parameters due to susceptibility to fiber dislocation, matrix overflow, lack of matrix material, and fiber damage [29]. On the other hand, discontinuous fiber-reinforced polymer composites like LFRP enable flexible printing and can be easily recycled and reused [1]. Moreover, fiber dislocation is minimized because of the discontinuity in the reinforcing fibers. The fiber strands are generally well dispersed within the matrix [39,40].

In this study, a new AM method was proposed to print LFRP parts using a pellet-based extrusion deposition process. Continuous fiber tows and thermoplastic pellets were used as feedstock materials. During the printing process, continuous fiber bundles were chopped into long fibers by shearing forces during extrusion, mixed with thermoplastic melt, and then deposited layer-by-layer on a print bed. The obtained LFRP samples were compared with SFRP and CFRP samples prepared by similar extrusion deposition methods used for LSAM. Both mechanical properties and microstructure were studied. A detailed comparison of fiber dispersion, distribution of fiber length and orientation, and fiber wetting condition was performed for the printed composite samples. The fiber impregnation process was further investigated. Large-scale composite parts with complex geometries were also fabricated to demonstrate the feasibility of the proposed AM method.

Experimental Procedure

Material Preparation. Commercially available polylactic acid (PLA) pellets (4043D by Filabot) were used in this study as the thermoplastic matrix material. 3K carbon fiber tows (3000 fibers in a bundle, AS4C by Hexcel) were used as the reinforcement fiber. The PLA was selected in this study due to its wide applications in AM as well as its relative low costs. The PLA pellets were dried in a vacuum oven at 85 °C for at least 4 h to eliminate moisture before three-dimensional (3D) printing as the presence of moisture could hydrolyze PLA in the melt phase, which in turn reduces its molecular weight and subsequent mechanical properties of the printed samples [41]. Thorough drying of PLA pellets also minimizes bubble formation during deposition [42]. Similarly, the carbon fiber tows were dried in a vacuum oven at 120 °C for at least 4 h to remove moisture and minimize the probability of fiber clumping during extrusion [43]. The PLA pellets and continuous fiber tows were directly used as feedstock materials in preparing LFRP and CFRP samples.

Short carbon fiber-reinforced PLA (fiber-PLA) pellets were used instead to prepare SFRP samples. The fiber-PLA pellets were prepared following the previously reported procedure [44,45]. The selected 3K carbon fiber tows were first chopped to 3.2 mm in length, and then 6 vol% fibers and PLA were dissolved in anhydrous dichloromethane (DCM) solvent (by Sigma-Aldrich) and mixed using a magnetic stirrer for 8 h. The mixture was then dried under a fume hood at ambient temperature and pelletized. The prepared fiber-PLA pellets were stored in a vacuum oven at 80 °C to minimize the presence of moisture [41] prior to fabrication.

Experimental Setup. A custom single-screw extruder with a print nozzle of 4 mm inner diameter in Fig. 1 was used to fabricate all the samples in this study, and it was controlled by a multi-axis machine (Galaxy G by Automated Precision Inc.) to follow a prespecified toolpath in three-dimensional space. A high torque motor was used to drive the extrusion process by controlling its rotation speed. An acrylic print bed was selected in this study for deposition due to its thermoplastic nature that promotes adhesion between deposited samples and substrates. The presence of thermally conductive carbon fibers made the temperature distribution more uniform during deposition, thus lowering warping of deposited composite samples. These helped make the acrylic print bed a viable substrate without requiring additional setup, e.g., a heated print bed.

Carbon fibers were fed through different processes as illustrated in Fig. 1 in preparing different types of composite samples. SFRP samples were obtained with the prepared fiber-PLA pellets directly used as the feedstock in Fig. 1(*a*). Pure PLA samples were also prepared by using PLA pellets in this study for comparison with composite samples. Continuous carbon fiber tows, if fed through a vent hole on the extruder as shown in Fig. 1(*b*), were chopped down into discontinuous long carbon fibers by extrusion induced shearing forces. The process is expected to incorporate long carbon fibers into deposited samples and thus additively fabricate LFRP samples. If the continuous carbon fiber tows were directly impregnated through the print nozzle [27,29] as shown in Fig. 1(*c*) instead of through the vent hole on the extruder, CFRP samples can be prepared.

During extrusion, the pellets were melted by a heater and mixed with carbon fibers as they were fed through the extruder and coextruded out through the print nozzle. The fiber-PLA mixture was then deposited layer-by-layer to print the composite sample. The material extrusion and deposition rates were controlled by the extruder screw rotation speed, as represented by revolutions per minute (RPM) at a given melt temperature. The extrusion process was expected to facilitate orientation of the reinforcing fibers in the print direction during deposition owing to shear and melt flow induced fiber alignment [46–48], which was further examined as described below.

Preliminary studies were first performed to find optimal printing parameters. The print temperature, layer thickness, material deposition rate, and print speed would affect the quality of the printed samples [29,49]. A print temperature of 190 °C was found to allow sufficient viscosity for the PLA melt to provide a drag force needed to coextrude carbon fibers at a wide range of extruder

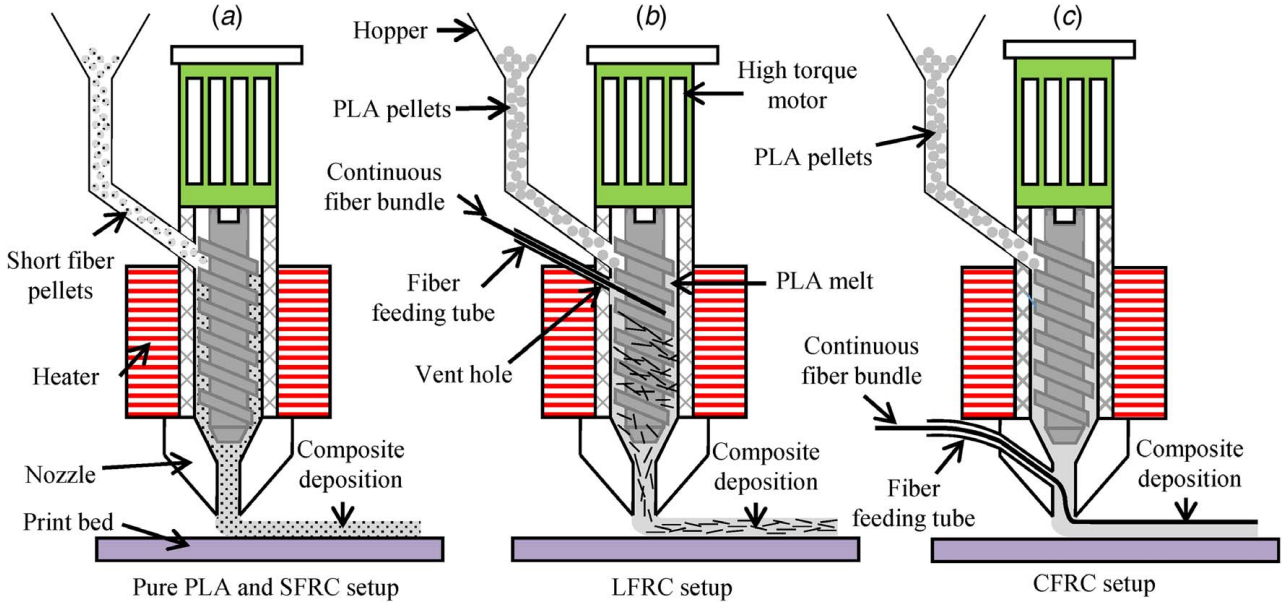

Fig. 1 Schematics of the AM setup in printing (*a*) SFRP, (*b*) LFRP, and (*c*) CFRP samples

RPMs and print speeds. A layer thickness of 1 mm was used to ensure sufficient contact pressure to avoid delamination between deposition layers [29]. The extruder screw's rotation speed was selected as 200 RPM, with a calibrated extruder material output rate, i.e., a deposition rate of 3.3 g/min, which is about six times higher than the deposition rates, e.g., 0.17–0.46 g/min [29], typically achieved by the filament-based FFF processes. It is worth noting that as the deposition rate was controlled by the extruder screw's rotation speed, the deposition rate can be easily scaled up to a higher value at a higher rotation speed, e.g., 833.3 g/min as reported in previous studies for LSAM [34]. The constant deposition rate of 3.3 g/min here was employed with a print speed of 200 mm/min. The print speed in this study denotes the traverse speed of the extrusion nozzle. Under these conditions, pure PLA, SFRP, LFRP, and CFRP samples were fabricated for mechanical tests and microstructural analyses. The feasibility of the proposed process was further demonstrated by printing large-scale composite samples with complex geometries at a higher deposition rate of 13.3 g/min.

Mechanical Testing and Microstructure Characterization. The printed samples were studied through mechanical testing and microscopic observation across their cross sections. Flexural strength and modulus of the additively fabricated composite samples were measured using three-point bending tests in Fig. 2 as they are closely related to fiber-matrix interfacial bonding [50].

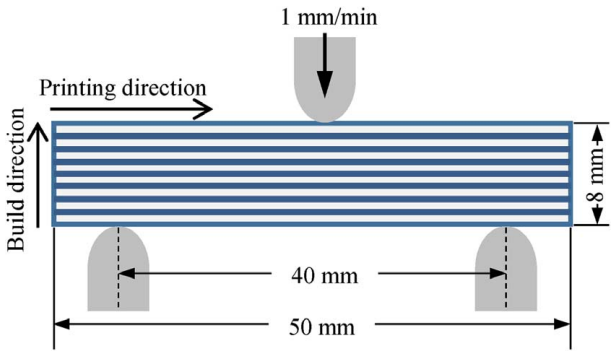

Fig. 2 Schematics of the three-point bending test setup

It should be noted that for better comparison, the pure PLA samples were also tested to measure their flexural properties. Same bending test conditions have been implemented for all additively fabricated pure PLA, SFRP, LFRP, and CFRP samples. Rectangular bars with dimensions of 50 mm × 8 mm × 8 mm were fabricated using the proposed setup with the aforementioned printing parameters. Flexural strength and modulus were determined using the three-point bending method on an Instron 5881 machine with a support span of 40 mm as shown in Fig. 2. Three specimens of each type of samples were tested at a cross-head speed of 1 mm/min.

To characterize fiber distribution within PLA matrix material, the additively fabricated composite parts were first cut using a low-speed diamond saw both perpendicular to the print direction to obtain transverse cross sections for studying fiber dispersion, and along the print direction to obtain longitudinal cross sections for studying fiber orientation. The cross sections were polished using resin bonded diamond discs between 220 and 1200 in grit size, followed by diamond films between 3 μm and 0.25 μm. The polished samples as well as fractured surfaces of the bending test samples were examined by scanning electron microscopy (SEM) on a Quanta 600F Environmental Scanning Electron Microscope. For SEM analyses, the samples were sputter coated with 25 nm platinum coating to improve image resolution and minimize charging of the sample. IMAGEJ software was used to analyze the void fraction on the polished transverse cross sections [16,26]. A Hirox Digital KH-8700 optical microscope was also used to examine the polished samples. It is worth noting that with adequate polishing, high transparency of the selected PLA matrix material facilitated characterization of reinforcing carbon fibers. To facilitate measurement of fiber length in the composite samples, the printed composite samples were repeatedly rinsed with DCM solvent until all the PLA matrix material was dissolved. The remaining carbon fibers were then used to characterize fiber length distribution through the analysis software IMAGEJ. The weight of the remaining carbon fibers was also measured. Once knowing the weight of the printed composite samples, carbon fiber volume fraction V_f can be obtained using [16,17,29,51]

$$V_f = \frac{W_f}{\rho_f}\left(\frac{1}{\frac{W_f}{\rho_f}+\frac{W_m}{\rho_m}}\right) \tag{1}$$

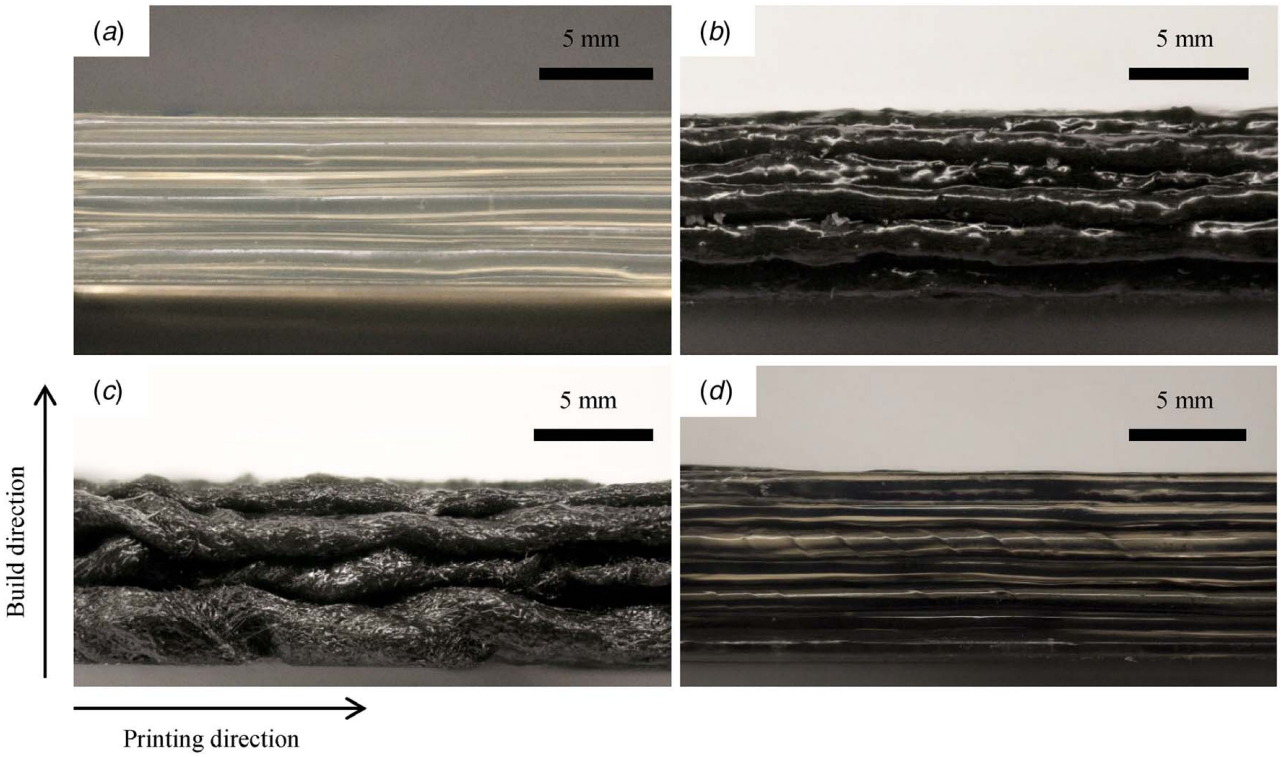

Fig. 3 Comparison of side views showing typical deposited layers of additively manufactured (*a*) pure PLA, (*b*) SFRP, (*c*) LFRP, and (*d*) CFRP samples

where W_f and W_m represent the weights of fiber reinforcements and matrix material, respectively. The densities of continuous carbon fiber reinforcements (ρ_f) and PLA matrix materials (ρ_m) were taken as 1.24 g/cm^3 and 1.78 g/cm^3, respectively, for the selected carbon fiber tows (AS4C by Hexcel) [52] and PLA pellets (4043D by Filabot) [53] in this study, where a constant 6 vol% of carbon fibers were maintained for all composite samples.

Results and Discussion

Morphology Comparison of the Printed Samples. Using the experimental setup described above, pure PLA, SFRP, LFRP, and CFRP samples were printed with their typical morphology shown in Fig. 3. Relatively large layer thickness and poor surface finish were observed for the printed samples. This is mainly due to the relatively large deposition rate (3.3 g/min) in this study compared with 0.17–0.46 g/min [29] typically used by fused filament fabrication processes, as well as the large layer thickness (1 mm) used in this study, as typically required for large-scale additive manufacturing. Decreasing material deposition rate or layer thickness may help improve print resolution and reduce layer variation; however, it would not be suitable for large-scale additive manufacturing.

Meanwhile, relatively large variation among deposition layers was observed for SFRP, LFRP, and CFRP samples printed under same conditions. Fiber-reinforced composites are more susceptible to fiber dislocation, pull-out, matrix overflow, and lack of matrix materials [29] during the printing processes. Difficulties in printing of composites increase [1] with an increase in fiber length. For the CFRP samples in Fig. 3(*d*), carbon fibers seen as dark phases were obviously non-uniformly distributed. The heterogeneity in fiber distribution could potentially lead to a higher degree of defects in the printed samples and thus decrease their mechanical properties. In contrast, with uniform darkness observed for both SFRP and LFRP samples in Fig. 3, fiber strands were expected to be well dispersed within matrix materials during the extrusion [39].

It should also be noted that a constant 1 mm layer thickness was used for all types of printed composite samples in Fig. 3, where a total of 8 layers were deposited during printing processes. However, due to variation among the deposited layers, particularly obvious in Fig. 3(*c*), some overflowing layers even completely covered previously deposited layers, resulting in seemingly different number of layers for different types of composite samples. This was found to be mainly due to the unique heterogeneity introduced by the discontinuous long fiber reinforcement in the LFRP samples. As further discussed below, a wide variation in carbon fiber length in the LFRP samples resulted in the most obvious variation between deposited layers and thus worse print resolution and surface anomalies in Fig. 3(*c*).

Microstructural Characterization. The microstructure of the printed composite samples was first compared through SEM examinations of polished transverse cross sections in Fig. 4. The carbon fibers were relatively uniformly distributed across the cross sections of the SFRP and LFRP samples. This showed a clear difference compared with the fiber distribution within the CFRP samples in Fig. 4(*c*), where continuous carbon fibers tended to concentrate within the transverse cross section due to drawing force [29,30]. On the other hand, a noticeable higher amount of voids were observed in the CFRP samples. A significant amount of voids were observed both around and within the carbon fiber bundle in Fig. 4(*c*), showing much worse fiber wetting conditions during printing processes. In contrast, for the SFRP and LFRP samples, the voids mainly formed within the polymer matrix with a few smaller voids also observed around carbon fiber. As shown in Fig. 5, the measured void fraction for the LFRP samples was slightly higher than that of the SFRP samples. The void fraction of the CFRP samples was much larger, over four times of that found in the LFRP samples.

The polished longitudinal cross sections were compared between different composite samples in Fig. 6. Compared with the SFRP samples in Fig. 6(*a*), slightly conglomerated fibers were observed within the LFRP samples as shown in Fig. 6(*b*), mainly caused by the drawing forces during deposition, which also contributed to the much more concentrated fiber bundles seen in the CFRP

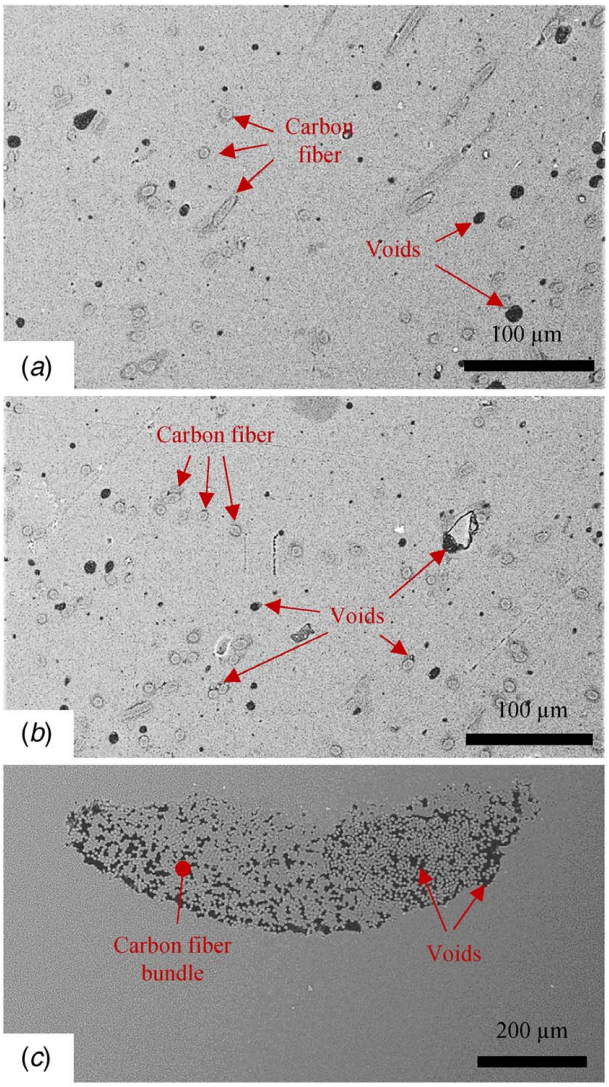

Fig. 4 SEM images of polished transverse cross sections of composite samples: (*a*) SFRP, (*b*) LFRP, and (c) CFRP

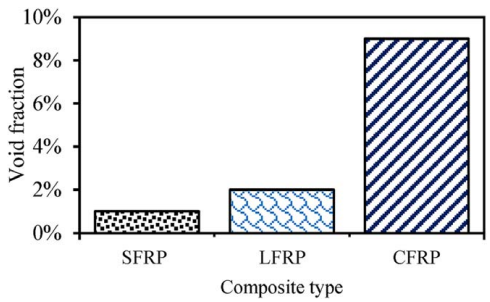

Fig. 5 Comparison of void fraction within the printed SFRP, LFRP, and CFRP samples

samples in Fig. 6(*c*). However, due to the discontinuity in fibers for the SFRP and LFRP samples, the fiber distribution was less affected by the drawing forces and showed a higher degree of uniformity.

Carbon Fiber Dispersion. Fiber dispersion within composite samples directly correlates with mechanical properties [54]. Thus, the dispersion of carbon fibers in Fig. 4 was also quantified to evaluate the fiber distribution across the transverse cross section. Following the previous fiber dispersion measurement process [40], the carbon fibers were first converted to dots in an *X*–*Y* coordinate system, where *Xi* and *Yi* represented the transverse direction and build direction, respectively. The cross section was segregated into small grids (32 × 32), called quadrants. The number (*N*) of the marked fiber dots falling into each quadrant (*Xi*,*Yi*) were then counted. The count distribution can then be used to quantify the degree of fiber distribution uniformity across the transverse cross section by mapping as shown in Figs. 7(*a*)–7(*c*). A relatively uniform distribution of carbon fibers was observed for both SFRP and LFRP samples. In contrast, significant peak values shifting toward the top region of the deposition bead were observed for CFRP samples.

Carbon Fiber Length. The actual fiber lengths within fiber-reinforced composite samples play a very important role in the obtained mechanical properties, which typically increased with an increase in fiber length. Thus, the lengths of all carbon fibers incorporated in the printed LFRP and SFRP samples were measured after dissolving and removing the PLA matrix materials via DCM. The results are summarized in Fig. 8(*a*) to characterize the distribution of carbon fiber length. The measured numbers of fibers were normalized by the total number of all measured carbon fibers, so the vertical axis represented the percentage of fiber length within a corresponding range. The cumulative distribution of fiber length is also summarized in Fig. 8(*b*) to facilitate comparison of LFRP and SFRP samples. As a very low degree of fiber breakage was observed within the printed CFRP samples, their reinforcing fiber length was not explicitly characterized due to the continuity nature.

Compared with LFRP samples, a narrower range of fiber length distribution is observed for SFRP samples in Fig. 8(*a*). An average of 0.3 mm fiber length was found in the printed SFRP samples with a maximum of 3.01 mm and a minimum of 6 μm measured. About 80% of fiber length was found smaller than 0.4 mm for SFRP samples as measured from the cumulative fiber distribution in Fig. 8(*b*). For the LFRP samples, a more diverse distribution of fiber length is observed in Fig. 8(*a*). An average of 20.1 mm fiber length was obtained with a maximum of 32.0 mm and a minimum of 4 μm measured. As measured from Fig. 8(*b*), less than 1% fiber length in LFRP samples was smaller than 5.0 mm.

Carbon Fiber Orientation. To study the fiber orientation distribution, a window of 1350 μm × 1350 μm was first selected at three different longitudinal cross sections on three different samples for each type of composites. The fiber orientation angle with respect to the printing direction was obtained for all the fibers within the window. The printing direction was defined as 0 deg, and the build direction was defined as 90 deg. The distributions of carbon fiber orientation within the SFRP and LFRP samples are summarized in Fig. 9(*a*). The numbers of fibers were normalized by the total number of all measured carbon fibers, so the vertical axis represented the percentage of fibers measured within a corresponding orientation range. The cumulative distributions of fiber orientation were also included as shown in Fig. 9(*b*) to facilitate comparison between LFRP and SFRP samples. No fiber orientation was explicitly characterized for the CFRP samples as nearly all continuous carbon fibers were aligned along the printing direction seen in Fig. 6(*c*), attributed to the drawing force during deposition.

A relatively more diverse distribution of fiber orientation was observed for the SFRP samples in Fig. 9(*a*). Only about 46% of the fibers were oriented within 10 deg from the printing direction as measured in Fig. 9(*b*). With almost no drawing forces applied on the short fibers within the SFRP samples, fiber alignment was expected to be governed by extrusion induced shearing. For the LFRP samples, 68% of the fibers were aligned within 10 deg and 86% oriented within 30 deg from the printing direction. This was expected to be attributed to a combination of shearing induced fiber alignment during extrusion and drawing forces during deposition. Compared with the shorter fibers of the SFRP samples, the

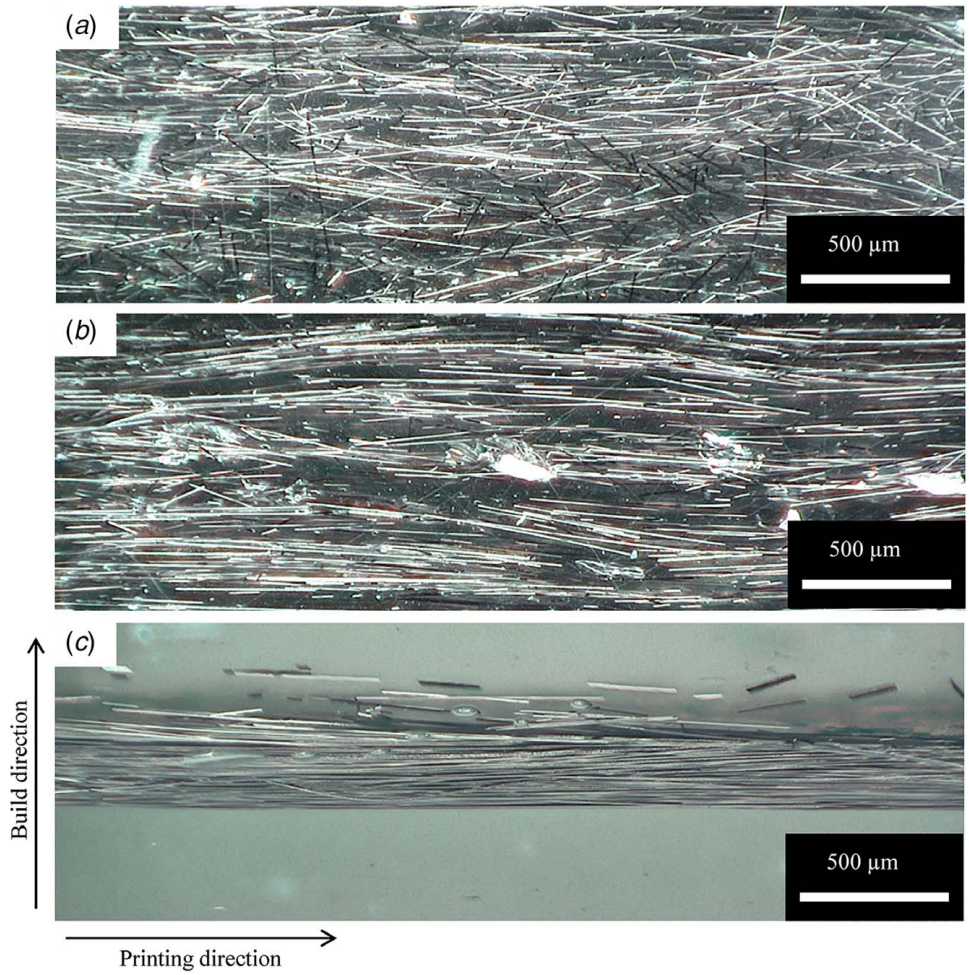

Fig. 6 Optical microscopic images of polished longitudinal cross sections of a deposited bead of the printed (*a*) SFRP, (*b*) LFRP, and (*c*) CFRP samples

increased fiber length within the LFRP samples also increased the viscous drag force between fibers and polymers, promoting alignment of the carbon fiber phases under shearing.

Fiber Wetting and Impregnation Process Analysis. Fiber-matrix interfacial bonding is one major factor governing the performance of fiber-reinforced composites [27,29], which is closely related to fiber wetting conditions. Compared with the SFRP and LFRP samples in Fig. 4, the much higher amount of voids observed both around and within carbon fiber bundle in Fig. 4(*c*) revealed much worse fiber wetting conditions during printing of the CFRP samples. The difference is believed to be attributed to different fiber impregnation processes during printing of the SFRP, LFRP, and CFRP samples.

For the SFRP samples, fiber impregnation is affected by the fiber-PLA pellets used for printing [34]. A thorough fiber and PLA mixing procedure was followed in this study during preparing these pellets, resulting in a high degree of fiber impregnation. On the other hand, an in situ fiber impregnation process [16] was implemented in printing LFRP and CFRP samples to improve fabrication efficiency by directly using continuous fibers and PLA pellets as feedstock materials. With the high deposition rate implemented, the impregnation time was very short. Only a few minutes took from supplying feedstock materials to depositing composites, much shorter than that used in preparing fiber-PLA pellets (8 h) in this study. However, compared with LFRP, the impregnation time was even shorter for CFRP. Similar to the previous studies in printing CFRP [27,29], the continuous carbon fiber tows were directly fed through the print nozzle in Fig. 1(*c*). The short impregnation time limited the amount of PLA flowing into the continuous carbon fiber bundles before deposition, thus yielding worse fiber wetting conditions. For the LFRP samples, as the carbon fiber tows and PLA pellets were nearly fed together as shown in Fig. 1(*b*), the relatively longer-time mixing processes during extrusion promoted fiber impregnation into PLA melt. Fiber impregnation rate, affecting the impregnation process, is also believed to be different between LFRP and CFRP samples. As shown in Fig. 10, it will take longer time for the PLA melt to flow into the continuous fiber network of CFRP compared with the long, discontinuous fiber network within LFRP.

For the poor fiber wetting conditions observed for the CFRP samples in Fig. 4(*c*), it is hypothesized that this is related to fiber impregnation mechanisms during the extrusion process. The cross section of the carbon fiber bundle in Fig. 10 is shown in Fig. 11. At the meso-scale in Figs. 11(*a*)–11(*c*), melt flow will penetrate through the carbon fiber network under pressure. The impregnation at this stage is expected to be determined by melt flowrate. A higher pressure is expected to achieve a higher melt flowrate and facilitate impregnation, yielding a better fiber-matrix interface condition [16]. A lowered viscosity, e.g., achieved at a higher melt temperature [29], will also improve melt flowrate and improve impregnation quality. With sufficient PLA melt flow around carbon fibers in Fig. 11(*c*), fiber-PLA adhesion will then be determined by the single fiber wetting process at the micro-scale as shown in Fig. 11(*d*). For a given polymer composition, e.g., PLA in this study, the wettability of a single carbon fiber at the micro-scale is affected by slip velocity between moving fibers and melt flow [55] in Fig. 10 and is typically characterized by a dynamic

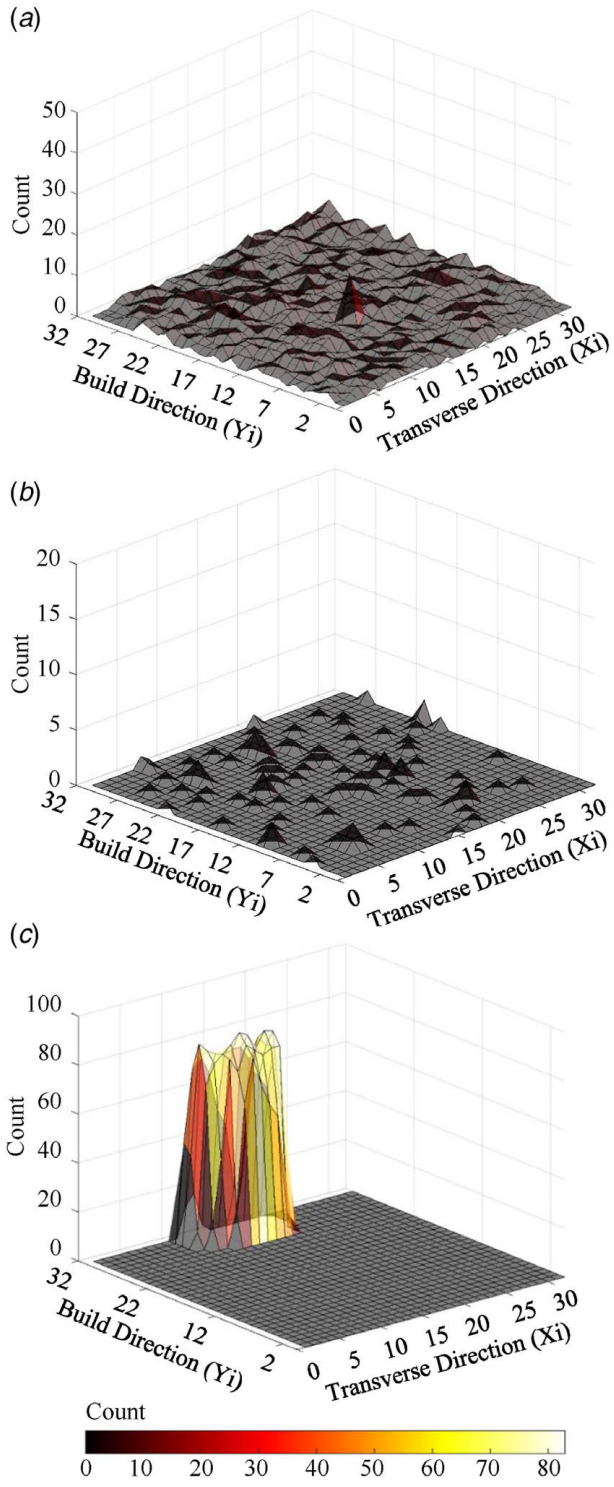

Fig. 7 Comparison of carbon fiber dispersion mapping across the transverse cross sections between (*a*) SFRP samples, (*b*) LFRP samples, and (c) CFRP samples

contact angle (θ) on the fiber surface as shown in Fig. 11(*d*). A relatively short impregnation time and a low impregnation rate limit the degree of impregnation that can be reached for the printed CFRP samples, possibly still at the stage shown in Fig. 11(*b*), resulting in the poor wetting conditions of the fiber bundle in Fig. 4(*c*). A further increased impregnation time at a higher impregnation rate will improve the degree of impregnation and thus fiber wetting conditions. With a sufficiently long impregnation time and a high impregnation rate, the degree of impregnation within the printed LFRP samples will then be mainly affected by the single fiber wetting condition that may create nucleation sites for some residual voids around single carbon fibers or combined voids around fiber clusters seen in Figs. 4(*b*) and 11(*c*).

Mechanical Properties. The mechanical properties of the printed composite samples were compared via three-point bending tests, where three samples were tested for each type. The measured stress–strain curves are plotted in Fig. 12, where the typical results for each type of composite samples are shown. The PLA samples were also measured and included for comparison. As expected, with no fiber reinforcement, the PLA samples showed the lowest mechanical strength. The measured flexural modulus and strength are summarized in Fig. 13. With an increase in reinforcing fiber length as measured in Fig. 8, a steady increase in average flexural strength was observed in the printed SFRP, LFRP, and CFRP samples compared with that of pure PLA samples. Attributed to the nature of continuous fiber reinforcements, the CFRP samples exhibited the highest improvement, about 52% stronger than their PLA counterparts. It is worth noting that although the average flexural strength of LFRP samples was lower than that of CFRP samples, the actual flexural strength values of the LFRP samples could fluctuate anywhere from a moderate improvement over the PLA samples, all the way up to almost being the same as the CFRP samples. Such obvious variation was partially attributed to the relatively large variation between deposited layers of the LFRP samples seen in Fig. 3. Meanwhile, as shown in fiber length distribution in Fig. 8, a wide range of fiber length was observed for the LFRP samples, ranging from 4 μm to 32 mm, which would introduce more inconsistencies in the mechanical performance [1,15]. In comparison, this phenomenon was less prominent for the SFRP samples with consistently small reinforcing fiber length seen in Fig. 8.

On the other hand, the average flexural modulus of the LFRP samples was found to be comparable to that of the CFRP samples, 49% over the PLA samples and 9% higher than the SFRP samples. The high modulus of the printed LFRP samples could be attributed largely to highly oriented long carbon fibers measured in Fig. 9. In addition, well dispersed long discontinuous carbon fiber networks in Fig. 7 not only improve fiber wetting as seen in Fig. 4 but also formed a strong fibrous reinforcement, more effectively stiffening the composites, compared with the typically concentrated continuous carbon fibers within the printed CFRP samples [29,30].

Previous studies [1,15,56] showed that the stiffness of fiber-reinforced composites increased with an increase in the aspect ratio of reinforcing fibers until a critical aspect ratio was reached. Beyond that, the stiffness remained essentially constant irrespective of further increase in the length of reinforcing fibers. Hence, the comparable modulus of the LFRP and CFRP composites could be attributed to the fact that a critical fiber aspect ratio $(l/d)_c$ was reached in the LFRP samples, which is determined by

$$\left(\frac{l}{d}\right)_c = \frac{\sigma_{fu}}{2\tau} \tag{2}$$

where l and d are the carbon fiber length and diameter, respectively. σ_{fu} denotes the ultimate tensile strength of the carbon fibers, and τ represents the interfacial shear strength between the fiber and the PLA matrix material. For the selected carbon fiber tows (AS4C by Hexcel) [52], d and σ_{fu} were 7 μm and 4.7 GPa, respectively. With an estimated interfacial shear strength of 5.0 MPa [40] for the extrusion process, a critical carbon fiber length of 3.3 mm needs to be achieved for selected composite compositions in this study. As measured in Fig. 8(*b*) above, only less than 1% of fibers in the LFRP samples had length smaller than 3.3 mm, suggesting that a majority of carbon fibers were effectively strengthening and stiffening the printed LFRP samples [1], thus yielding high modulus comparable to that of the CFRP samples seen in Fig. 13.

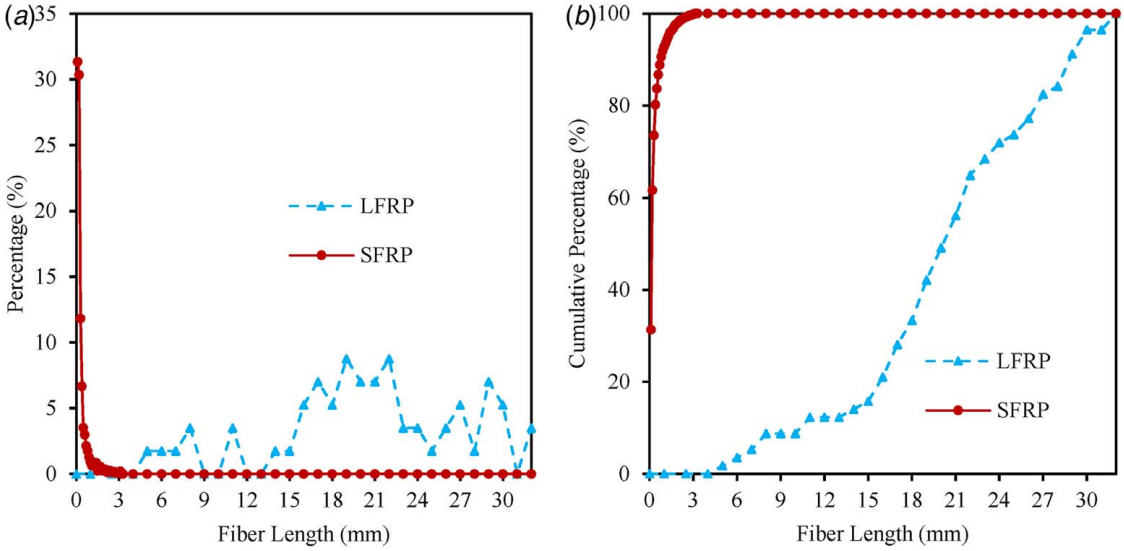

Fig. 8 Fiber length comparison between printed LFRP and SFRP samples: (*a*) distribution of fiber length and (*b*) cumulative distribution of fiber length

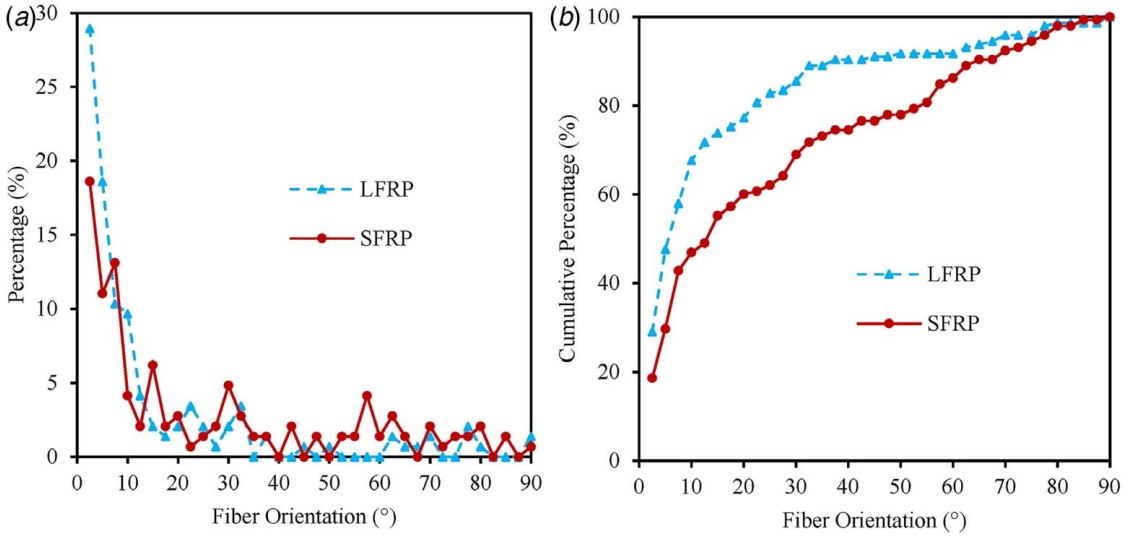

Fig. 9 Fiber orientation comparison between printed LFRP and SFRP samples: (*a*) distribution of fiber orientation and (*b*) cumulative distribution of fiber orientation

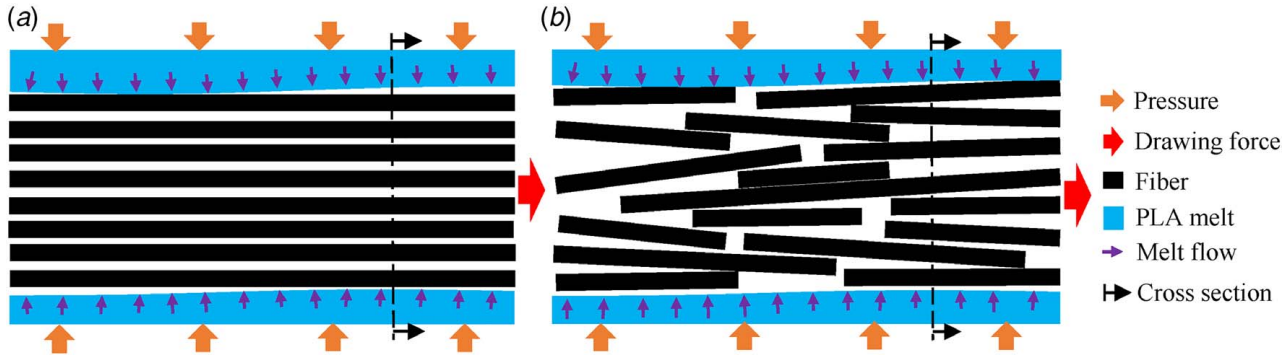

Fig. 10 Comparison of fiber impregnation processes between (*a*) CFRP and (*b*) LFRP samples

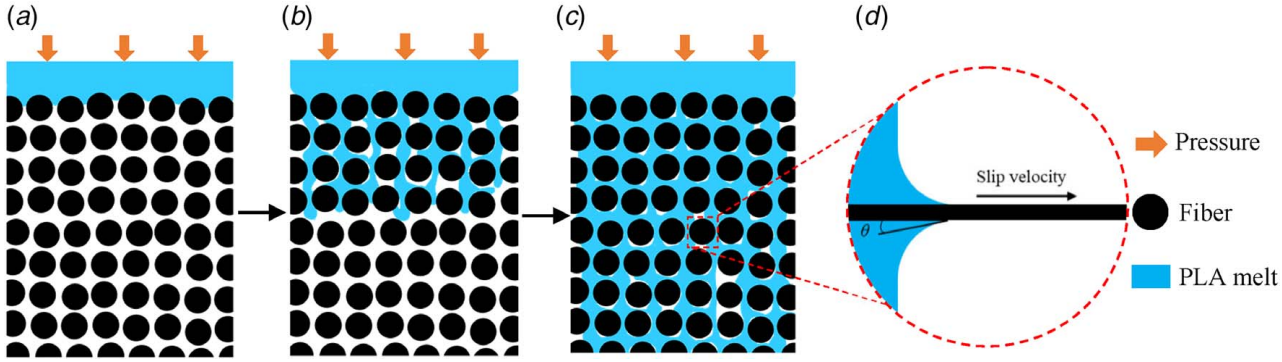

Fig. 11 Schematics of the cross section of carbon fiber bundle and impregnation mechanisms as a combined PLA penetration of the carbon fiber network at the meso-scale from (*a*–*c*) and the single fiber wetting process in (*d*)

Meanwhile, the large fiber length variation was observed to increase fiber entanglement for the LFRP samples. In the examination of the carbon fiber strands, it was found that the singled, untangled fibers were most likely to be less than 170 μm in length, while the fibers exceeding 440 μm were likely to be entangled into slight conglomerates. With highly oriented carbon fibers, if fewer long fibers were entangled in the printed samples, a better dispersed fiber reinforcement network would lead to higher mechanical properties. However, with a majority of long carbon fibers present in the LFRP samples as seen in Fig. 8, carbon fibers had a high tendency to entangle and accumulate as slight conglomerates as shown in Fig. 6(*b*). The increased heterogeneity weakened the reinforcing effects of long fibers, leading to a larger variation in the flexural strength and modulus seen in Fig. 13. It is worth noting that such heterogeneity would make it challenging to accurately calculate composite properties and compare with experimental measurements. It is expected that multi-scale numerical modeling approaches [57–59] will provide better solutions to evaluate the effects of microstructure including fiber length as well as its variation on mechanical and even thermal properties for different types of composite samples.

Further examination of the fractured surfaces of bending test samples in Fig. 14 helped reveal the damage mechanisms. Relatively clean fractured surfaces were observed for the SFRP samples in Fig. 14(*a*) and the LFRP samples in Fig. 14(*b*). These are found in Figs. 14(*d*) and 14(*e*) to be mainly attributed to polymer matrix cracking and fiber pull-out due to fiber-matrix debonding. For the CFRP samples in Fig. 14(*c*), the damage was also found to be governed by polymer matrix cracking and fiber pull-out. Specifically, the fiber pull-out in the CFRP samples was found to be mainly attributed to delamination between fiber and matrix in Fig. 14(*f*), possibly due to the very poor fiber wetting conditions seen in Fig. 4(*c*). Meanwhile, obvious fiber breakage was also observed.

Demonstration of Three-Dimensional Printed Carbon Fiber-Reinforced Polymer Composites. The applications of the proposed method in printing composite parts were demonstrated through the obtained structures shown in Fig. 15. A print speed of 200 mm/min and a deposition rate of 13.3 g/min were used. The AM method proposed here as demonstrated in Figs. 15(*a*) and 15(*b*), to the best of our knowledge, for the first time, facilitated additive manufacturing of complex composite parts reinforced with long carbon fiber. With high deposition rates, the proposed method enables fabrication of large-format part with shorter amounts of time compared with the traditional filament-based FFF processes. The wing-rib structure shown in Fig. 15(*c*) was finished within 2 h, attributed to the high deposition rates employed (13.3 g/min or 0.8 kg/h), which normally would take days to print by filament-based FFF processes. Meanwhile, the average material cost was just around $10/kg, much lower than the typical filament-based FFF processes that may even increase the manufacturing cost of seemingly low-cost thermoplastics to $100/kg [34]. However, it is also worth noting that due to larger variation of incorporated long fibers, the printed LFRP parts exhibited a relatively lower print resolution and higher surface roughness, compared with the obtained SFRP and CFRP parts in Figs. 15(*d*) and 15(*e*). Thus, future studies will be conducted to improve the proposed AM method in

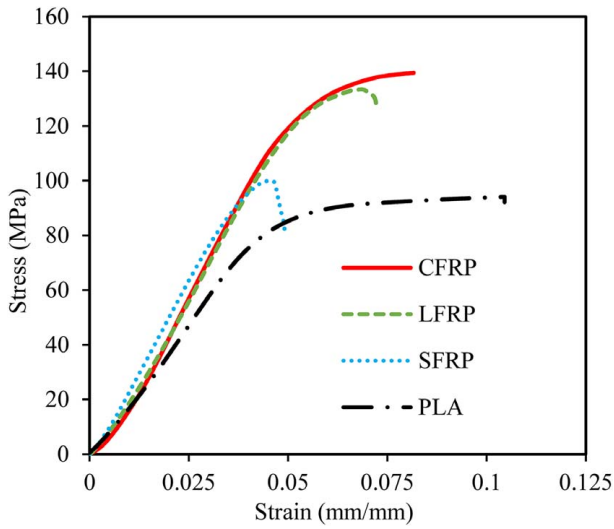

Fig. 12 Measured typical stress–strain curves through three-point bending tests on additively manufactured PLA, SFRP, LFRP, and CFRP samples

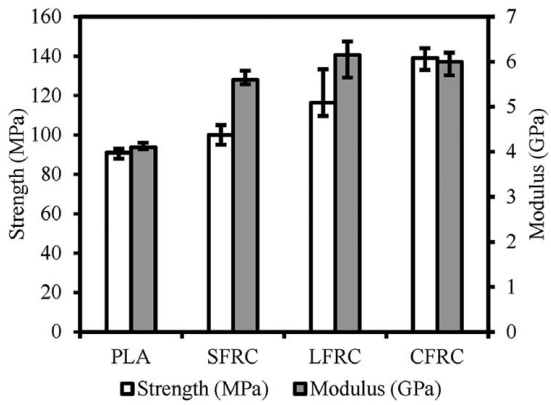

Fig. 13 Comparison of measured flexural strength and modulus between pure PLA, SFRP, LFRP, and CFRP samples

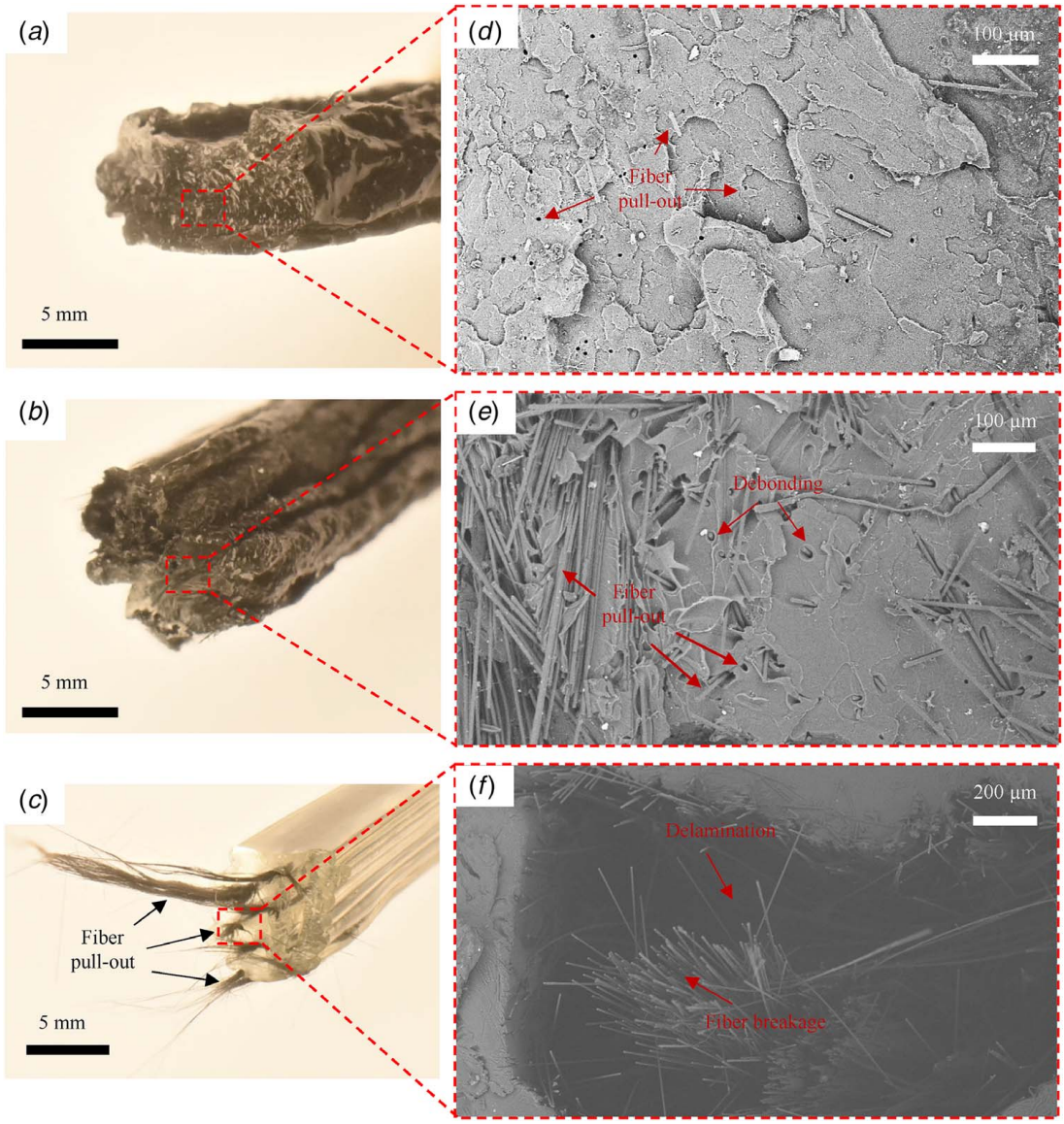

Fig. 14 Optical microscopic images of fractured surfaces for (*a*) SFRP, (*b*) LFRP, and (*c*) CFRP samples and close-up views of SEM images for (*d*) SFRP, (*e*) LFRP, and (*f*) CFRP samples

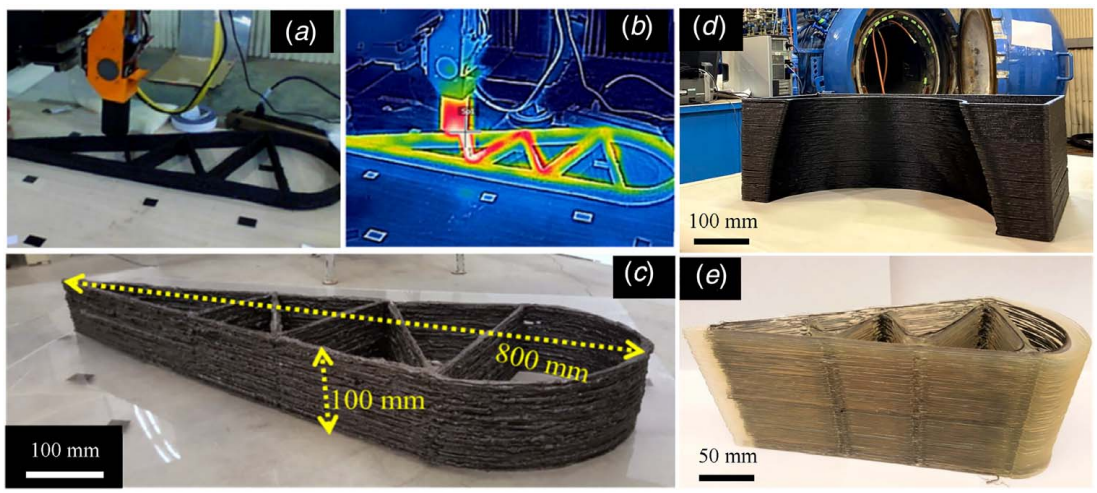

Fig. 15 Demonstration of the printed composite components at a deposition rate of 13.3 g/min and a print speed of 200 mm/min: (*a*) the LFRP printing process, (*b*) thermal imaging of the LFRP layer-by-layer deposition process, (*c*) the printed LFRP wing-rib part, (*d*) a Cessna 414 nose-cone mold structure printed with SFRP, and (*e*) a wing-rib part printed with CFRP

fabricating LFRP samples. Meanwhile, post-processing procedure, e.g., machining and polishing [60–62], can be used to improve the surface finish of large-scale printed final products. The successfully printed composite parts demonstrated here have proven the feasibility of the proposed method in fabricating structural components for LSAM, particularly with LFRP, potentially capable of replacing metal parts in aerospace and automotive industries.

Conclusion

In this study, a pellet-based extrusion deposition method was used to prepare and compare SFRP, LFRP, and CFRP parts for large-scale additive manufacturing. In particular, a novel AM method was proposed to directly print long carbon fiber-reinforced polymer composites. This method used continuous carbon fiber tows and thermoplastic pellets as feedstock materials. The printed LFRP samples exhibited flexural modulus comparable to the CFRP samples. This was found to be attributed to highly aligned and relatively well distributed long fibers with an average length of 20.1 mm, much longer than the estimated critical fiber length of 3.3 mm for the material composition in this study. However, a wide variation of fiber length led to a large variation of flexural strength and modulus observed in the LFRP samples. With much lower void fraction, the void pattern in SFRP and LFRP samples was found to be notably different from that of the CFRP samples printed under the same conditions. This is believed to be attributed to a longer impregnation time and a higher impregnation rate achieved by the discontinuous carbon fiber networks within the SFRP and LFRP samples. The feasibility of the proposed AM method was further demonstrated through successfully printed large-scale complex structures. These results showed the high potentials of the proposed method in additive manufacturing of large-scale, high-strength fiber-reinforced composites.

Acknowledgment

The authors acknowledge the funding support by the Intelligent Systems Center at the Missouri University of Science and Technology for the research work presented in this paper. The technical assistance of Charng-Yuh Lee in preparing samples during the experiments is also much appreciated.

Conflict of Interest

There are no conflicts of interest.

Data Availability Statement

The datasets generated and supporting the findings of this article are obtainable from the corresponding author upon reasonable request. The authors attest that all data for this study are included in the paper.

References

[1] Ning, H., Lu, N., Hassen, A. A., Chawla, K., Selim, M., and Pillay, S., 2020, "A Review of Long Fibre Thermoplastic (LFT) Composites," Int. Mater. Rev., **65**(3), pp. 164–188.
[2] Hartness, T., Husman, G., Koenig, J., and Dyksterhouse, J., 2001, "The Characterization of Low Cost Fiber Reinforced Thermoplastic Composites Produced by the DRIFT^{TM} Process," Compos. Part A: Appl. Sci. Manuf., **32**(8), pp. 1155–1160.
[3] Tanabe, D., Kubohori, F., Imamura, S., Jiang, H., Nishiyabu, K., and Kurashiki, T., 2016, "Continuous Tape Layup Molding of CFRTP Using Near-Infrared Heating and High Frequency Induction Roller Heating," 17th European Conference on Composite Materials, ECCM 2016, Munich, Germany, June 26–30, p. 126913.
[4] Rakhshbahar, M., and Sinapius, M., 2018, "A Novel Approach: Combination of Automated Fiber Placement (AFP) and Additive Layer Manufacturing (ALM)," J. Compos. Sci., **2**(3), p. 42.
[5] Composites World, 2015, "Fabrication Methods." https://www.compositesworld.com/articles/fabrication-methods-2015, Accessed October 20, 2019.
[6] Crosky, A., Grant, C., Kelly, D., Legrand, X., and Pearce, G., 2015, "Fibre Placement Processes for Composites Manufacture," *Advances in Composites Manufacturing and Process Design*, P. Boisse, ed., Woodhead Publishing, Sawston, UK, pp. 79–92.
[7] Marian, J., Venturini, G., Hansen, B. L., Knap, J., Ortiz, M., and Campbell, G. H., 2010, "Finite-Temperature Extension of the Quasicontinuum Method Using Langevin Dynamics: Entropy Losses and Analysis of Errors," Model. Simul. Mater. Sci. Eng., **18**(1), p. 15003.
[8] Degenhardt, R., 2017, "Stability of Composite Shell–Type Structures," *Stability and Vibrations of Thin Walled Composite Structures*, H. Abramovich, ed., Woodhead Publishing, Sawston, UK, pp. 253–428.
[9] CompositesWorld, 2017, "Reconfigurable Tooling: Revolutionizing Composites Manufacturing." https://www.compositesworld.com/articles/reconfigurable-tooling-revolutionizing-composites-manufacturing, Accessed October 20, 2019.
[10] Hoa, S. V., 2017, "Factors Affecting the Properties of Composites Made by 4D Printing (Moldless Composites Manufacturing)," Adv. Manuf. Polym. Compos. Sci., **3**(3), pp. 101–109.
[11] Rihaczek, G., Klammer, M., Basnak, O., Petrš, J., Grisin, B., Dahy, H., Carosella, S., and Middendorf, P., 2020, "Curved Foldable Tailored Fiber Reinforcements for Moldless Customized Bio-Composite Structures. Proof of Concept: Biomimetic NFRP Stools," Polymers (Basel), **12**(9), p. 2000.
[12] Zhai, Y., Lados, D. A., and Lagoy, J. L., 2014, "Additive Manufacturing: Making Imagination the Major Limitation," JOM, **66**(5), pp. 808–816.
[13] Moreno Nieto, D., Casal López, V., and Molina, S. I., 2018, "Large-Format Polymeric Pellet-Based Additive Manufacturing for the Naval Industry," Addit. Manuf., **23**, pp. 79–85.
[14] Yang, S. W., and Chin, W. K., 1999, "Mechanical Properties of Aligned Long Glass Fiber Reinforced Polypropylene. II: Tensile Creep Behavior," Polym. Compos., **20**(2), pp. 207–215.
[15] Chawla, K. K., 1989, "Composite Materials Science and Engineering," Composites, **20**(3), p. 286.
[16] Liu, T., Tian, X., Zhang, Y., Cao, Y., and Li, D., 2020, "High-Pressure Interfacial Impregnation by Micro-Screw In-Situ Extrusion for 3D Printed Continuous Carbon Fiber Reinforced Nylon Composites," Compos. Part A: Appl. Sci. Manuf., **130**, p. 105770.
[17] Luo, M., Tian, X., Shang, J., Zhu, W., Li, D., and Qin, Y., 2019, "Impregnation and Interlayer Bonding Behaviours of 3D-Printed Continuous Carbon-Fiber-Reinforced Poly-Ether-Ether-Ketone Composites," Compos. Part A: Appl. Sci. Manuf., **121**, pp. 130–138.
[18] Toll, S., and Aronsson, C. G., 1992, "Notched Strength of Long- and Short-Fibre Reinforced Polyamide," Compos. Sci. Technol., **45**(1), pp. 43–54.
[19] Vu-Khanh, T., and Denault, J., 1992, "Toughness of Reinforced Ductile Thermoplastics," J. Compos. Mater., **26**(15), pp. 2262–2277.
[20] Yasuda, H., Chiba, Y., and Ishikawa, M., 2011, "Effect of the Glass Fiber Length on the Mechanical Properties of Long Glass Fiber Reinforced Polyphenylene Sulfide," J. Polym. Eng., **31**(5), pp. 427–434.
[21] Ning, F., Cong, W., Hu, Y., and Wang, H., 2017, "Additive Manufacturing of Carbon Fiber-Reinforced Plastic Composites Using Fused Deposition Modeling: Effects of Process Parameters on Tensile Properties," J. Compos. Mater., **51**(4), pp. 451–462.
[22] Dudek, P., 2013, "FDM 3D Printing Technology in Manufacturing Composite Elements," Arch. Metall. Mater., **58**(4), pp. 1415–1418.
[23] Farahani, R. D., Dalir, H., Le Borgne, V., Gautier, L. A., El Khakani, M. A., Lévesque, M., and Therriault, D., 2012, "Direct-Write Fabrication of Freestanding Nanocomposite Strain Sensors," Nanotechnology, **23**(8), p. 085502.
[24] Ferreira, R. T. L., Amatte, I. C., Dutra, T. A., and Bürger, D., 2017, "Experimental Characterization and Micrography of 3D Printed PLA and PLA Reinforced With Short Carbon Fibers," Compos. Part B: Eng., **124**, pp. 88–100.
[25] Papon, E. A., and Haque, A., 2019, "Fracture Toughness of Additively Manufactured Carbon Fiber Reinforced Composites," Addit. Manuf., **26**, pp. 41–52.
[26] Justo, J., Távara, L., García-Guzmán, L., and París, F., 2018, "Characterization of 3D Printed Long Fibre Reinforced Composites," Compos. Struct., **185**, pp. 537–548.
[27] Li, N., Li, Y., and Liu, S., 2016, "Rapid Prototyping of Continuous Carbon Fiber Reinforced Polylactic Acid Composites by 3D Printing," J. Mater. Process. Technol., **238**, pp. 218–225.
[28] Yao, X., Luan, C., Zhang, D., Lan, L., and Fu, J., 2017, "Evaluation of Carbon Fiber-Embedded 3D Printed Structures for Strengthening and Structural-Health Monitoring," Mater. Des., **114**, pp. 424–432.
[29] Tian, X., Liu, T., Yang, C., Wang, Q., and Li, D., 2016, "Interface and Performance of 3D Printed Continuous Carbon Fiber Reinforced PLA Composites," Compos. Part A: Appl. Sci. Manuf., **88**, pp. 198–205.
[30] Matsuzaki, R., Ueda, M., Namiki, M., Jeong, T. K., Asahara, H., Horiguchi, K., Nakamura, T., Todoroki, A., and Hirano, Y., 2016, "Three-Dimensional Printing of Continuous-Fiber Composites by In-Nozzle Impregnation," Sci. Rep., **6**(1), p. 23058.
[31] Dutra, T. A., Ferreira, R. T. L., Resende, H. B., and Guimarães, A., 2019, "Mechanical Characterization and Asymptotic Homogenization of 3D-Printed Continuous Carbon Fiber-Reinforced Thermoplastic," J. Brazilian Soc. Mech. Sci. Eng., **41**(3), p. 133.
[32] Zhang, H., Liu, D., Huang, T., Hu, Q., and Lammer, H., 2020, "Three-Dimensional Printing of Continuous Flax Fiber-Reinforced

Thermoplastic Composites by Five-Axis Machine," Materials (Basel), **13**(7), p. 1678.
[33] Ye, W., Lin, G., Wu, W., Geng, P., Hu, X., Gao, Z., and Zhao, J., 2019, "Separated 3D Printing of Continuous Carbon Fiber Reinforced Thermoplastic Polyimide," Compos. Part A: Appl. Sci. Manuf., **121**, pp. 457–464.
[34] Duty, C. E., Kunc, V., Compton, B., Post, B., Erdman, D., Smith, R., Lind, R., Lloyd, P., and Love, L., 2017, "Structure and Mechanical Behavior of Big Area Additive Manufacturing (BAAM) Materials," Rapid Prototyp. J., **23**(1), pp. 181–189.
[35] Brenken, B., Barocio, E., Favaloro, A., Kunc, V., and Pipes, R. B., 2018, "Fused Filament Fabrication of Fiber-Reinforced Polymers: A Review," Addit. Manuf., **21**, pp. 1–16.
[36] Zhang, J., Zhou, Z., Zhang, F., Tan, Y., Tu, Y., and Yang, B., 2020, "Performance of 3D-Printed Continuous-Carbon-Fiber-Reinforced Plastics With Pressure," Materials (Basel), **13**(2), p. 471.
[37] Li, N., Link, G., and Jelonnek, J., 2020, "3D Microwave Printing Temperature Control of Continuous Carbon Fiber Reinforced Composites," Compos. Sci. Technol., **187**, p. 107939.
[38] Liu, T., Tian, X., Zhang, M., Abliz, D., Li, D., and Ziegmann, G., 2018, "Interfacial Performance and Fracture Patterns of 3D Printed Continuous Carbon Fiber With Sizing Reinforced PA6 Composites," Compos. Part A: Appl. Sci. Manuf., **114**, pp. 368–376.
[39] Balaji Thattaiparthasarathy, K., Pillay, S., Ning, H., and Vaidya, U. K., 2008, "Process Simulation, Design and Manufacturing of a Long Fiber Thermoplastic Composite for Mass Transit Application," Compos. Part A: Appl. Sci. Manuf., **39**(9), pp. 1512–1521.
[40] Yan, X., and Cao, S., 2018, "Structure and Interfacial Shear Strength of Polypropylene-Glass Fiber/Carbon Fiber Hybrid Composites Fabricated by Direct Fiber Feeding Injection Molding," Compos. Struct., **185**, pp. 362–372.
[41] Van den Oever, M. J. A., Beck, B., and Müssig, J., 2010, "Agrofibre Reinforced Poly (Lactic Acid) Composites: Effect of Moisture on Degradation and Mechanical Properties," Compos. Part A: Appl. Sci. Manuf., **41**(11), pp. 1628–1635.
[42] Park, H., Kim, B., Gim, J., Han, E., and Rhee, B., 2017, "A Study on the Entrapped Air Bubble in the Plasticizing Process," Annual Technical Conference—ANTEC, Conference Proceedings, Anaheim, CA, May 8–10, pp. 1635–1639.
[43] Pérez-Pacheco, E., Cauich-Cupul, J. I., Valadez-González, A., and Herrera-Franco, P. J., 2013, "Effect of Moisture Absorption on the Mechanical Behavior of Carbon Fiber/Epoxy Matrix Composites," J. Mater. Sci., **48**(5), pp. 1873–1882.
[44] Zhong, W., Li, F., Zhang, Z., Song, L., and Li, Z., 2001, "Short Fiber Reinforced Composites for Fused Deposition Modeling," Mater. Sci. Eng. A, **301**(2), pp. 125–130.
[45] Tekinalp, H. L., Kunc, V., Velez-Garcia, G. M., Duty, C. E., Love, L. J., Naskar, A. K., Blue, C. A., and Ozcan, S., 2014, "Highly Oriented Carbon Fiber-Polymer Composites via Additive Manufacturing," Compos. Sci. Technol., **105**, pp. 144–150.
[46] Moses, K. B., Advani, S. G., and Reinhardt, A., 2001, "Investigation of Fiber Motion Near Solid Boundaries in Simple Shear Flow," Rheol. Acta, **40**(3), pp. 296–306.
[47] Joung, C. G., Phan-Thien, N., and Fan, X. J., 2001, "Direct Simulations of Flexible Fibers," J. Non-Newton. Fluid Mech., **99**(1), pp. 1–36.
[48] Jeffery, G. B., 1922, "The Motion of Ellipsoidal Particles Immersed in a Viscous Fluid," Proc. R. Soc. A, Math. Phys. Eng. Sci., **102**(715), pp. 161–179.
[49] Tian, X., Liu, T., Wang, Q., Dilmurat, A., Li, D., and Ziegmann, G., 2017, "Recycling and Remanufacturing of 3D Printed Continuous Carbon Fiber Reinforced PLA Composites," J. Clean. Prod., **142**, pp. 1609–1618.
[50] Mehndiratta, A., Bandyopadhyaya, S., Kumar, V., and Kumar, D., 2018, "Experimental Investigation of Span Length for Flexural Test of Fiber Reinforced Polymer Composite Laminates," J. Mater. Res. Technol., **7**(1), pp. 89–95.
[51] Kabir, S. M. F., Mathur, K., and Seyam, A. F. M., 2020, "A Critical Review on 3D Printed Continuous Fiber-Reinforced Composites: History, Mechanism, Materials and Properties," Compos. Struct., **232**, p. 111476.
[52] Hexcel, 2019, "HexTow® Continuous Carbon Fiber." https://www.hexcel.com/Products/Carbon-Fiber/HexTow-Continuous-Carbon-Fiber, Accessed October 20, 2019.
[53] Filabot, 2019, "Pulverized Pla—4043D." https://www.filabot.com/products/pulverized-pla, Accessed October 20, 2019.
[54] McNally, D., 1977, "Short Fiber Orientation and Its Effects on the Properties of Thermoplastic Composite Materials," Polym. Plast. Technol. Eng., **8**(2), pp. 101–154.
[55] Qiu, S., Fuentes, C. A., Zhang, D., Van Vuure, A. W., and Seveno, D., 2016, "Wettability of a Single Carbon Fiber," Langmuir, **32**(38), pp. 9697–9705.
[56] Wang, Q., Jones, J., Lu, N., Johnson, R., Ning, H., and Pillay, S., 2018, "Development and Characterization of High-Performance Kenaf Fiber–HDPE Composites," J. Reinf. Plast. Compos., **37**(3), pp. 191–200.
[57] Dong, X., and Shin, Y. C., 2017, "Multi-Scale Modeling of Thermal Conductivity of SiC-Reinforced Aluminum Metal Matrix Composite," J. Compos. Mater., **51**(28), pp. 3941–3953.
[58] Dong, X., and Shin, Y. C., 2018, "Multi-Scale Genome Modeling for Predicting Fracture Strength of Silicon Carbide Ceramics," Comput. Mater. Sci., **141**, pp. 10–18.
[59] Dong, X., and Shin, Y. C., 2018, "Predictions of Thermal Conductivity and Degradation of Irradiated SiC/SiC Composites by Materials-Genome-Based Multiscale Modeling," J. Nucl. Mater., **512**, pp. 268–275.
[60] Lužanin, O., Movrin, D., and Plan, M., 2013, "Experimental Investigation of Extrusion Speed and Temperature Effects on Arithmetic Mean Surface Roughness in FDM-Built Specimens," J. Technol. Plast., **38**(2), pp. 179–190.
[61] Gajdoš, I., Spišák, E., Kaščák, Ľ, and Krasinskyi, V., 2015, "Surface Finish Techniques for FDM Parts," *Materials Science Forum*, vol. 818, pp. 45–48.
[62] Singh, R., Singh, S., Singh, I. P., Fabbrocino, F., and Fraternali, F., 2017, "Investigation for Surface Finish Improvement of FDM Parts by Vapor Smoothing Process," Compos. Part B: Eng., **111**, pp. 228–234.